Dalton Transactions

PAPER

View Article Online
View Journal | View Issue

Cite this: *Dalton Trans.*, 2016, **45**, 13944

Coupling with a narrow-band-gap semiconductor for the enhancement of visible-light photocatalytic activity: preparation of $Bi_2O_xS_{3-x}/Nb_6O_{17}$ and application to the degradation of methyl orange†

Gang Yan,[a] Hongfei Shi,[a] Huaqiao Tan,*[a] Wanbin Zhu,[b] Yonghui Wang,*[a] Hongying Zang[a] and Yangguang Li*[a]

Received 13th June 2016,
Accepted 3rd August 2016

DOI: 10.1039/c6dt02338j

www.rsc.org/dalton

A series of 2D sheet $Bi_2O_xS_{3-x}/Nb_6O_{17}$ (Bi/Nb) heterostructure photocatalysts were synthesized through a facile hydrothermal vulcanization method between Bi^{3+} exchanged $K_4Nb_6O_{17}$ and thiourea (NH_2CSNH_2). XRD results confirm that the heterostructures were composed of $Bi_2O_xS_{3-x}$ and Nb_6O_{17}. HRTEM indicates that $Bi_2O_xS_{3-x}$ was successfully intercalated into layers of $K_4Nb_6O_{17}$. Such large interfacial contacts can be beneficial to the transfer and separation of photogenerated charge carriers. Thus the composites exhibit good photocatalytic performance for the degradation of methyl orange (MO) under visible light irradiation ($\lambda > 400$ nm), which is superior to that of both precursors, pure Bi_2S_3 and $K_4Nb_6O_{17}$. Radical capture tests reveal that photogenerated holes h^+ and $^{\bullet}O_2^-$ play important roles in the photodegradation of MO. And based on the UV-visible diffuse reflectance spectra (DRS) and the band gap of the semiconductors, the mechanism of the enhanced visible light photocatalytic activity of these composites has been proposed.

Introduction

Photocatalysis, as a "green" and energy saving method to completely eliminate environmental pollutants, has aroused tremendous interest.[1–4] In this field, a fundamental issue is the construction of highly efficient photocatalysts. Semiconductor hetero-structures with staggered alignment band gaps can not only improve the separation of photogenerated charge carriers, but also widen the light absorption when a narrow band gap component is used.[5–12] Thus these heterostructured semiconductors usually show more preferable photocatalytic performance, and are considered as highly efficient photocatalysts, especially heterostructures with a layered structure. Two-dimensional (2D) layered materials have attracted considerable attention because of their high specific surface area, short charge transport distance and tunable hybrid properties from mediating the composition of the hosts and the intercalated guests.[13] They can be used as a nano-reactor and support, which limits the growth and combination of semiconductors in the inter-layers, thus fabricating more favorable heterostructures owing to the relatively large interfacial contact.

Based on the above mentioned points, $K_4Nb_6O_{17}$ has attracted our attention for its good photocatalytic applications in water splitting[14] and the degradation of pollutants.[15–20] It is well known that $K_4Nb_6O_{17}$ possesses a unique layered structure with two distinct interlayer spaces of hydrated K^+ and unhydrated K^+ ions.[21,22] The hydrated K^+ ions can be exchanged with various metal ions, organic molecules and metal complexes. A series of intercalation composites, such as noble metal nanoparticles,[15] transition metal sulfides (CdS,[16] Cu_2S,[17] PbS[18]), halogen/AgX,[19–21] organic dyes,[23,24] metalloporphyrins[25] and metal-poly (pyridyl) chelates,[26] intercalated into $K_4Nb_6O_{17}$ have been synthesized, which indicates that $K_4Nb_6O_{17}$ is a good support for its cation-exchange and swelling properties. However, to date the intercalation of some layered structures into the interlayers of $K_4Nb_6O_{17}$ to form a 2D sheet composite has been largely unexplored.

Bismuth(III)-based semiconductors, such as BiOX (X = Cl, Br and I),[27] Bi_2WO_6,[28,29] Bi_2MoO_6,[30–36] $BiVO_4$ [37] and $Bi_2O_{3-x}S_x$

[a]*Key Laboratory of Polyoxometalate Science of Ministry of Education, Department of Chemistry, Northeast Normal University, Ren Min Street No. 5268, Changchun, Jilin, 130024, People's Republic of China. E-mail: tanhq870@126.com, wangyh319@nenu.edu.cn, liyg658@nenu.edu.cn*

[b]*State Key Laboratory of Applied Optics, Changchun Institute of Optics, Fine Mechanics and Physics, Chinese Academy of Sciences, Changchun 130033, P. R. China*

† Electronic supplementary information (ESI) available: SEM, TEM, the relationship between $(ahv)^2$ and photon energy (hv). See DOI: 10.1039/c6dt02338j

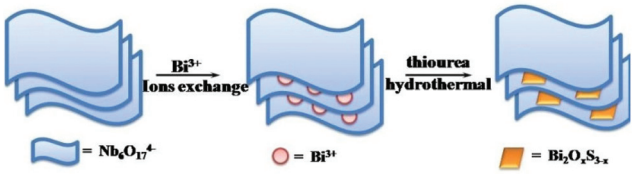

Scheme 1 Schematic view of the preparation procedure of heterostructure Bi/Nb composites.

(x = 0–3),[38] recently have been demonstrated to exhibit excellent photocatalytic performance. These compounds usually possess a layered structure, and can be regarded as a composition of a cationic [$Bi_2O_2^{2+}$] layer and different anions.[38] By controlling the species and the amounts of anions, the band gaps of these bismuth(III)-based semiconductors can be adjusted over a large range. For example, nanosized Bi_2O_3 possesses a large band gap, E_g = 2.8 eV, while Bi_2S_3 has a smaller band gap of 1.3 eV. By controlling the amounts of oxygen and sulfur in $Bi_2O_{3-x}S_x$ (x = 0–3), a series of [$Bi_2O_2^{2+}$]-containing compounds, such as Bi_2O_2S and $Bi_4O_4S_3$, can be formed band gaps ranging from 1.3 eV–2.8 eV.[38] However, compared to Bi_2O_3 and Bi_2S_3, [$Bi_2O_2^{2+}$]-containing $Bi_2O_{3-x}S_x$ has been seldom explored.

Herein, we used propylamine intercalated Pr-NH_3^+-Nb_6O_{17} as a precursor and through Bi^{3+} exchange, controlled hydrolysis and vulcanization, a series of 2D sheet composite photocatalysts, $Bi_2O_xS_{3-x}/Nb_6O_{17}$, have been synthesized using a facile hydrothermal reaction between Bi^{3+} exchanged $K_4Nb_6O_{17}$ and thiourea (NH_2CSNH_2), as illustrated in Scheme 1. With an increase in the thiourea added, the visible light absorption of the hybrid composites is improved gradually. Photocatalytic experiments reveal that the $Bi_2O_xS_{3-x}/Nb_6O_{17}$ composites show good photocatalytic performance for the degradation of methyl orange (MO) under visible light irradiation (λ > 400 nm). When 0.1 g of thiourea (NH_2CSNH_2) was added, the sample Bi/Nb-0.1 g exhibited the highest photocatalytic performance. 50 ml of 20 ppm methyl orange, MO, can be almost completely photodegraded (50 mg of photocatalyst) in 30 min under visible light irradiation, which is more efficient than both precursors, Bi_2S_3 and $K_4Nb_6O_{17}$.

Experimental

Materials

Niobium pentoxide (Nb_2O_5), potassium hydroxide (KOH), propylamine ($CH_3CH_2CH_2NH_2$), bismuth nitrate pentahydrate ($Bi(NO_3)_3{\cdot}5H_2O$), thiourea (NH_2CSNH_2), and nitric acid (HNO_3) were purchased from Aladdin Chemical Reagent Co., Ltd and were used as received without any further purification. Distilled water was also used in all experiments.

Preparation of $K_4Nb_6O_{17}$

2 g of Nb_2O_5 powder was dispersed in 70 ml of 1 mol L^{-1} KOH solution under vigorous stirring. Then the white suspension was put into a 100 mL Teflon-lined stainless autoclave and heated at 200 °C for 48 h. The product was separated using filtration, washed with distilled water and ethanol, and dried at 80 °C. And then 2 g of $K_4Nb_6O_{17}$ powder was added into 80 mL of 2 mol L^{-1} HCl solution, and stirred at 65 °C for 12 hours. The H^+ exchange product was collected using filtration, washed with distilled water, and ethanol, and dried at 85 °C under vacuum. Propylamine intercalated Pr-NH_3^+-Nb_6O_{17} was synthesized *via* the reaction of the above H^+-Nb_6O_{17} with a 50% volume ratio of propylamine in aqueous solution and stirred at 45 °C for 3 days. After that period, the sample was centrifuged, washed and dried. This material was designated as Pr-NH_3^+-Nb_6O_{17}.

Preparation of the photocatalyst

0.5 g of Pr-NH_3^+-Nb_6O_{17} was stirred with 30 ml of 1 mol L^{-1} $Bi(NO_3)_3{\cdot}5H_2O$ solution at ambient temperature for 24 h. After centrifugation, the Bi^{3+} exchanged product was dissolved in 50 mL of distilled water. Then, a specific amount of thiourea was added to the above solution. The pH of the mixed solution was adjusted to 7 with KOH solution. The composite $Bi_2O_xS_{3-x}/Nb_6O_{17}$ (detonated as Bi/Nb) was prepared through the hydrothermal reaction of the above solution at 180 °C for 24 h. The product was washed with water and ethanol 3 times and dried at 60 °C for 12 h. A series of $Bi_2O_xS_{3-x}/Nb_6O_{17}$ composites were prepared, and the final products were named Bi/Nb-0 g, Bi/Nb-0.02 g, Bi/Nb-0.05 g, Bi/Nb-0.1 g and Bi/Nb-0.3 g, respectively (0 g to 0.3 g indicates the mass of thiourea added). The pure Bi_2S_3 photocatalyst was obtained under the same conditions without the Bi^{3+} exchanged product.

Characterization

X-ray diffraction (XRD) data of samples were acquired on a Bruker AXS D8 Focus with filtered Cu-Kα radiation (λ = 1.54056 Å). A JEOL JSM 4800F SEM coupled with an energy-dispersive X-ray (EDX) spectrometer was used to characterize the sample morphology. UV-vis diffuse reflectance spectra (DRS) of the samples were collected with a UV-2600 UV-Vis spectrophotometer (Shimadzu), with $BaSO_4$ used as the reference and with an integrating sphere. High-resolution TEM (transmission electron microscopy) images were obtained using an FEI Tecnai G2 operated at 200 kV. XPS was carried out on an ESCALABMKII spectrometer with an Al-Kα (1486.6 eV) achromatic X-ray source.

Photocatalytic activity

The photocatalytic activities of the as-prepared samples were evaluated through the degradation of methyl orange (MO) solution using a 300 W Xe lamp as the light source with a 400 nm cut-off filter, and a self-made glass vessel with a water-cooling jacket as a reactor. The distance between the irradiation light source and the mixture solution was 15 cm. Prior to irradiation, a suspension solution containing 50 mg of photocatalyst and 50 mL of MO solution (20 ppm, pH = 2) was stirred in the dark for an hour to ensure that adsorption–desorption equilibrium between the organic molecules and the catalyst surface was reached. 2.0 mL of the reaction solution

was taken at given time intervals, centrifuged, and examined using a XinMao UV-vis spectrometer UV-7502 at a maximum absorption wavelength of 506 nm.

Photoelectrochemical measurements

The variations in the photoinduced current density with time (*i–t* curve) of the prepared photoelectrodes were measured with a CHI Electrochemical Workstation (CHI 660E, Shanghai Chenhua, China). The photoelectrodes (1 × 1 cm^2), Hg/Hg_2Cl_2, and platinum foil were used as the working, reference and counter electrodes, respectively. ITO (indium tin oxide)-coated glass, as the working electrode, was ultrasonically cleaned in deionized water and acetone successively. The photocatalyst powder was dispersed in alcohol solution (10 mg mL^{-1}) to produce slurry. And then the slurry was coated on the conductive surface of the ITO glass and dried in air at 60 °C. The photoelectrochemical measurements were conducted in 0.5 M Na_2SO_4. The *i–t* curves were measured at a −0.6 V bias potential. A 300 W Xe illuminator (Peking Ceaulight, CEL-HXF300) with a 400 nm UV-IR cut-off filter was used as the visible light source. The electrodes were irradiated from the back side (ITO substrate/semiconductor interface).

Results and discussion

XRD analysis

The XRD patterns of Bi_2S_3, the Bi/Nb hybrid composites and $K_4Nb_6O_{17}$ are shown in Fig. 1. The diffraction peaks at 23.00°, 27.58°, 31.551° and 46.20° can be assigned to $K_4Nb_6O_{17}$ with the standard PDF card (JCPDS 53-0780). This means that $K_4Nb_6O_{17}$ has been successfully synthesized. With the exchange of propylamine and Bi^{3+}, the diffraction peaks from Pr-NH_3^+-Nb_6O_{17} and Bi^{3+}-Nb_6O_{17} show shifts obviously, indicating the successful intercalation of propylamine and Bi^{3+}. When thiourea is not added, the hydrothermal product Bi/Nb-0 g exhibits a new diffraction peak at 29.30°, which can be attributed to Bi_2O_3 (JCPDS 65-3319). The peak from Bi_2O_3 in Bi/Nb-0 g shows a little shift compared to JCPDS 65-3319, which might be caused by the interaction of Bi_2O_3 and Nb_6O_{17} layers. With an increase in the thiourea added, the main diffraction peak of Bi_2O_3 (29.38°) was gradually shifted to Bi_2S_3 (28.60°), which means that a solid solution $Bi_2O_xS_{3-x}$ has been formed. When 0.3 g of thiourea was added, the characteristic peaks at 28.60° and 24.93° could be attributed to Bi_2S_3 (JCPDS 17-0320), indicating the formation of a Bi_2S_3/Nb_6O_{17} composite.

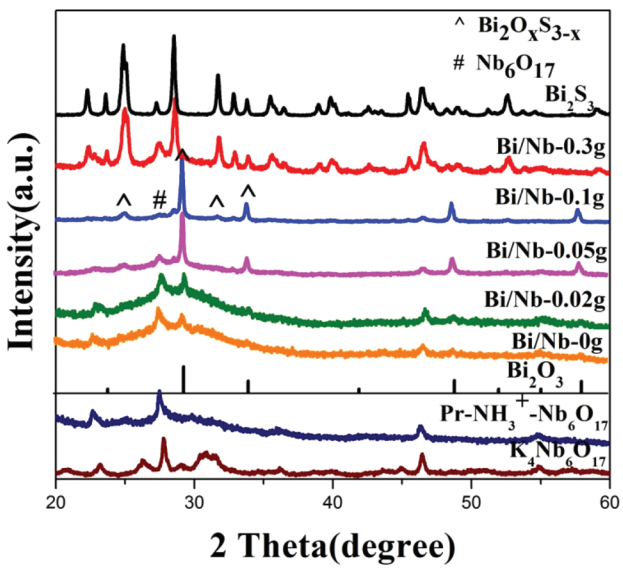

Fig. 1 XRD patterns of the Bi/Nb composites, Bi_2S_3, Bi_2O_3 and $K_4Nb_6O_{17}$.

SEM and TEM analysis

The morphology and microstructure of the Bi/Nb composites were further characterized using scanning electron microscopy (SEM) and transmission electron microscopy (TEM). As shown in Fig. 2a, the large thin sheets with a size of about 200–400 nm can be assigned to Nb_6O_{17}. In the interlayer space of Nb_6O_{17}, $Bi_2O_xS_{3-x}$ nanosheets with sizes ranging from 150 nm to 200 nm were obviously observed, which indicates the combination of $Bi_2O_xS_{3-x}$ and Nb_6O_{17} to form a 2D sheet composite. Such large interfacial contacts might be beneficial for the transfer and the separation of photogenerated charge carriers. Fig. 2b presents a HRTEM image of Bi/Nb-0.1 g. The clear lattice diffraction fringes with lattice plane distances of 0.31 nm can be assigned to $Bi_2O_xS_{3-x}$. This value is between 0.31180 nm (the interval of the Bi_2S_3 211 lattice plane) and 0.30369 nm (the interval of the Bi_2O_3 111 lattice plane), which further indicates the formation of a solid solution of $Bi_2O_xS_{3-x}$. This result was consistent with the results from XRD. Although Bi_2S_3 and Bi_2O_3 have similar chemical compositions, identical chemical states and anions possessing an approximately similar radius and electronegativity, reporting of this solid solution $Bi_2O_xS_{3-x}$ is scarce. Fig. 2c–f show the SEM elemental mapping of Bi/Nb-0.1 g. The Nb, S, and Bi elements were homogeneously distributed over the whole composite, indicating the combination of $Bi_2O_xS_{3-x}$ and Nb_6O_{17}. Fig. 2g shows the energy-dispersive X-ray (EDX) spectrum of Bi/Nb-0.1 g. The atom percentages of elements reveal that the ratio of Bi and S was about 1/1. Therefore, the chemical formula of $Bi_2O_xS_{3-x}$ in Bi/Nb-0.1 g can be assigned as Bi_2OS_2. In addition, the TEM of Bi/Nb-0.3 g is shown in Fig. S3.† Some Bi_2S_3 nanorods co-existed with the Bi_2S_3/Nb_6O_{17} composite, which indicates the dissolution of Bi ions as more thiourea was added. That might be related to the photocatalytic performance decrease for Bi/Nb-0.3 g.

XPS analysis

XPS was employed to investigate the surface composition and chemical state of the Bi/Nb composite. The characteristic peaks at about 532 eV, 440 eV, 205 eV and 160 eV can be assigned to O 1s, Bi 4d, Nb 3d, Bi 4f and S 2p respectively, indicating the presence of Bi, Nb, O, and S elements in Bi/Nb-0.1 g (Fig. 3a). A typical high-resolution XPS spectrum of Bi 4f and

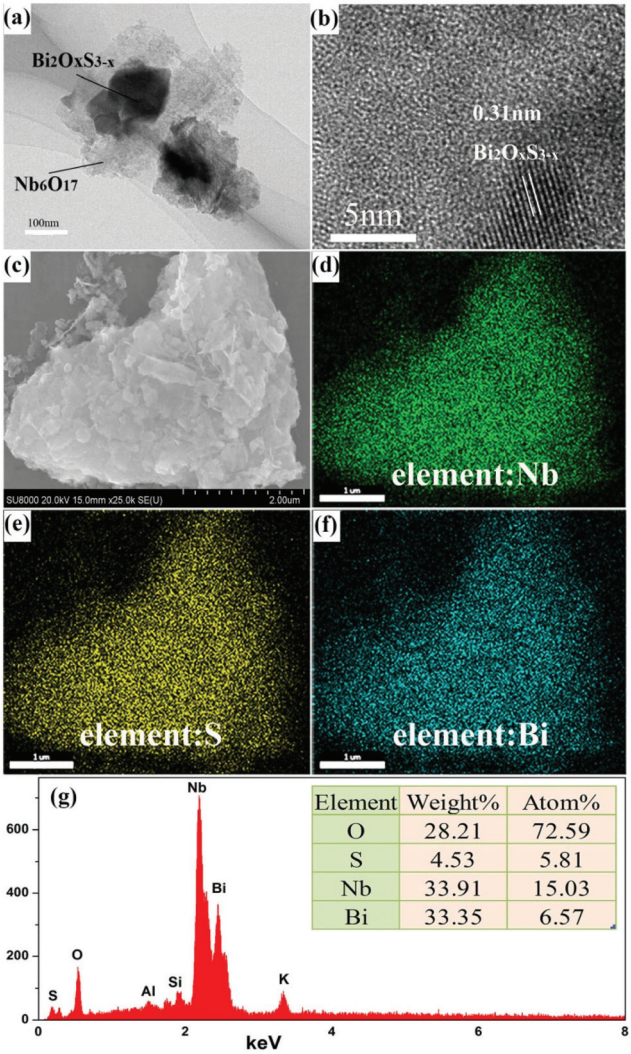

Fig. 2 (a) TEM and (b) HRTEM images of Bi/Nb-0.1 g; (c) SEM elemental mapping of the (d) Nb element, (e) S element and (f) Bi element; and (g) the energy-dispersive X-ray (EDX) spectrum – the Si and Al peaks originate from the substrate, and the K peak is from the unhydrated K^+ ions which cannot be exchanged.

S 2p for Bi/Nb-0.1 g is shown in Fig. 3b. There is partial overlapping of the peaks of Bi 4f5/2 and S 2p1/2, thus leading to a broad peak at about 163 eV. This peak can be split into three peaks. The peak at 164.0 eV can be assigned to S 2p1/2, which is consistent with that of Bi_2S_3.[39] The peaks at 163.6 eV and 158.8 eV are attributed to Bi 4f5/2 and Bi 4f7/2 from Bi–O.[40] In addition, the two peaks at 162.8 eV and 157.6 eV can be assigned to the binding energies of Bi 4f5/2 and Bi 4f7/2 from Bi–S.[40] Binding energies of Nb 3d5/2 and Nb 3d3/2 were observed at 206.5 eV and 209.3 eV, which indicates Nb in a +5 valence state (Fig. 3c).[41] The O 1s peak can also be split into three peaks at 529.6 eV, 531.5 eV and 532.7 eV (Fig. 3d), which are attributed to O–Bi,[42] O–Nb[43] and O–H,[44] respectively. In a word, the XPS results further confirm the combination of $Bi_2O_xS_{3-x}$ and Nb_6O_{17} to form a 2D sheet composite Bi/Nb.

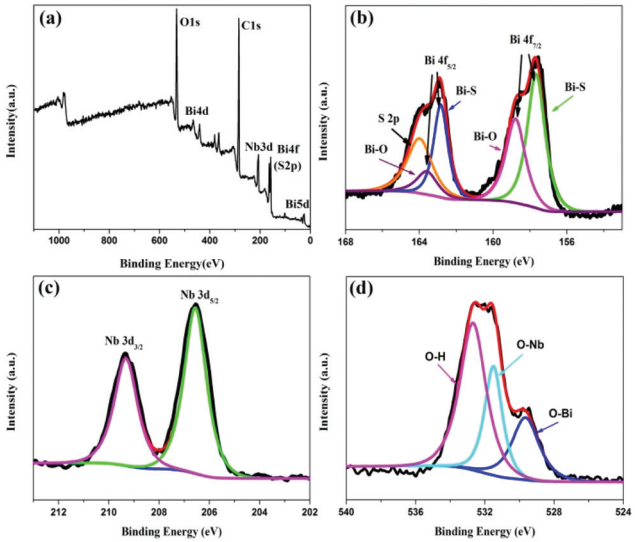

Fig. 3 XPS spectra of the Bi/Nb-0.1 g sample: (a) survey spectrum, (b) Bi 4f and S 2p, (c) Nb 3d, and (d) O 1s.

Optical properties

Fig. 4 exhibits the UV-visible diffuse reflectance spectra (DRS) of $K_4Nb_6O_{17}$, Bi_2S_3 and the Bi/Nb composites over the range of 200–900 nm. It can be seen that the absorption edge of pure $K_4Nb_6O_{17}$ was approximately 340 nm, which is consistent with the band gap of $K_4Nb_6O_{17}$ (3.7 eV). As thiourea was not added, Bi/Nb-0 g shows an obvious red shift in the light adsorption edge, which might be related to the formation of Bi_2O_3 in the interlayers of Nb_6O_{17}. With an increase in the thiourea added, the adsorption of the Bi/Nb composites in visible light was gradually enhanced. As shown in Fig. 4, Bi/Nb-0.1 g shows remarkable light adsorption in the range of 400–900 nm. This can be attributed to the narrow band gap and large absorption coefficient of Bi_2OS_2. When more thiourea was added, the

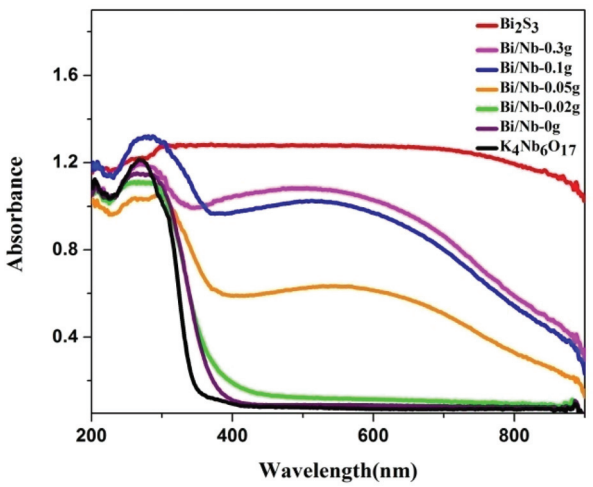

Fig. 4 UV-visible diffuse reflectance spectra (DRS) of $K_4Nb_6O_{17}$, Bi_2S_3 and the Bi/Nb composites.

light adsorption of the Bi/Nb composites in visible light changed slowly, which indicated that Bi/Nb-0.1 g and Bi/Nb-0.3 g possess similar band gaps. As shown in Fig. S4,† the band gaps of Bi/Nb-0.1 g and Bi/Nb-0.3 g are both about 1.53 eV. The band gap of Bi/Nb-0.3 g is slightly larger than that of pure Bi_2S_3 (1.38 eV), which might be caused by the size effect of Bi_2S_3 and the combination with Nb_6O_{17}.

Photocatalytic activity measurements

The photocatalytic activities of pure Bi_2S_3 and the Bi/Nb composites were assessed through the photodegradation of MO under visible light irradiation (λ > 400 nm). As shown in Fig. 5a, the blank and the control experiments using $K_4Nb_6O_{17}$ as a photocatalyst reveal that MO shows negligible degradation under visible light irradiation. Bi/Nb-0 g shows slight photocatalytic activity. 50 ml of 20 ppm MO can be degraded by about 5% in 30 min under visible light irradiation, with 50 mg of photocatalyst used. With an increase in the thiourea added to the system, the photocatalytic performance of the Bi/Nb composites is dramatically enhanced. As shown in Fig. 5a, about 55.8% of the MO was photodegraded using Bi/Nb-0.05 g as the photocatalyst, which can be compared with that by pure Bi_2S_3 (55%). Bi/Nb-0.1 g exhibits the best photocatalytic performance, and can degrade 99.8% of MO under the same conditions. That is obviously superior to both the precursors, $K_4Nb_6O_{17}$ and pure Bi_2S_3. As shown in Fig. 5b, the characteristic absorption peak of MO at 506 nm is rapidly reduced. After irradiation under visible light for about 30 min, MO was completely degraded. When Bi/Nb-0.3 g acted as catalyst, the degradation efficiency of MO was clearly decreased. That might be related to the composition of Bi/Nb-0.3 g. As the results of XRD and SEM indicate, Bi/Nb-0.3 g is composed of Bi_2S_3/Nb_6O_{17} composite and Bi_2S_3 nanorods. With the dissolution of Bi^{3+} and the formation of impurities of Bi_2S_3 nanorods in the Bi/Nb-0.3 g system, the efficient 2D sheet composite heterostructure is reduced or destroyed. Therefore, the photocatalytic activity is decreased compared to Bi/Nb-0.1 g. These results can be further confirmed using the reaction rate constant k. According to pseudo-first-order kinetics, $\ln(C_0/C) = kt$, the slope k is the apparent reaction rate constant. As shown in Fig. 5c, the apparent reaction rate constants k are 0.00125 min^{-1}, 0.00438 min^{-1}, 0.0244 min^{-1}, 0.0263 min^{-1}, 0.157 min^{-1} and 0.0464 min^{-1} for Bi/Nb-0 g and 0.02 g, pure Bi_2S_3, and Bi/Nb-0.05 g, 0.1 g and 0.3 g, respectively. It can be found that k for Bi/Nb-0.1 g is about 6.4 times and 3.4 times that for pure Bi_2S_3 and Bi/Nb-0.3 g. In order to investigate the stability and reusability of the catalysts, recycling experiments for Bi/Nb-0.1 g for the degradation of MO under visible light irradiation have been conducted. As shown in Fig. 5d, Bi/Nb-0.1 g does not show a significant loss in activity over three cycles. The MO degradation percentages are 99.8%, 95%, and 91%, for the first, second, and third runs respectively, which indicates that Bi/Nb-0.1 g possesses good photostability. The slight reduction in MO degradation percentages over different runs might come from a loss in catalyst in the process of recycling.

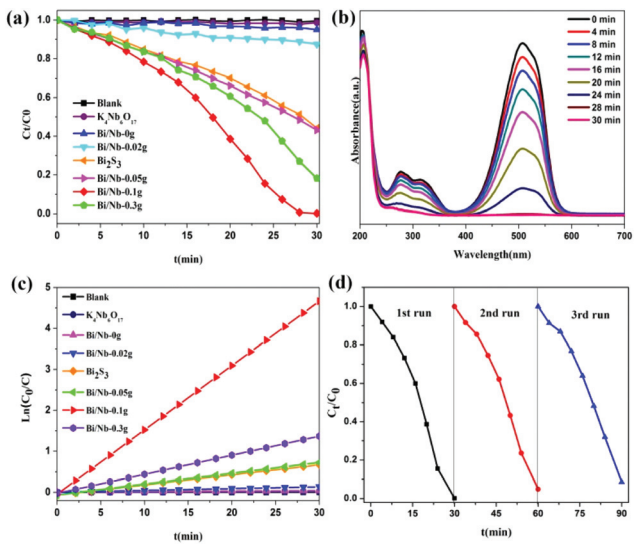

Fig. 5 (a) Photocatalytic degradation curves of different catalysts. (b) UV-Vis spectral changes during the photodegradation of MO mediated by Bi/Nb-0.1 g under visible light irradiation. (c) $Ln(C_0/C)$ *versus* time curves for MO degradation. (d) Recycling tests on the Bi/Nb-0.1 g sample for the degradation of MO under visible-light irradiation.

Photocurrent response and photocatalytic mechanism

In order to verify the enhanced visible light photocatalytic performance and the improvement in charge separation in the Bi/Nb composites, the transient photocurrent responses of $K_4Nb_6O_{17}$, Bi/Nb-0.1 g and pure Bi_2S_3 have been investigated. As shown in Fig. 6a, $K_4Nb_6O_{17}$ shows a negligible photocurrent response under visible light irradiation. Bi/Nb-0.1 g and pure Bi_2S_3 have a clear reproducible photocurrent response, when the light was switched on and off. This means that as $Bi_2O_xS_{3-x}$ was intercalated into the layered Nb_6O_{17}, the visible light photocatalytic performance of Nb_6O_{17} was largely improved. The photocurrent density of Bi/Nb-0.1 g, 1.817×10^{-4} mA cm^{-2}, was 1.2 times higher than that of pure Bi_2S_3 (1.521×10^{-4} mA cm^{-2}), implying that the charge separation in Bi/Nb-0.1 g was also significantly enhanced compared to that in pure Bi_2S_3. These results are consistent with those from the

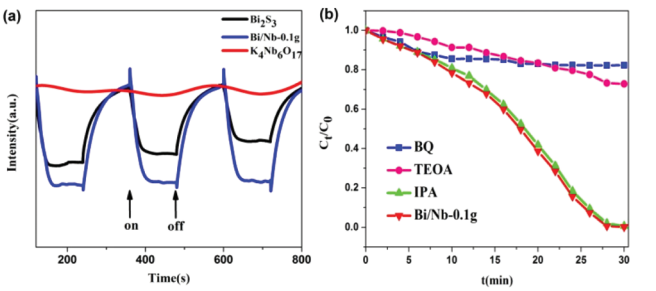

Fig. 6 (a) Photocurrent response tests of $K_4Nb_6O_{17}$, Bi/Nb-0.1 g and Bi_2S_3. (b) Photocatalytic degradation of MO over the Bi/Nb-0.1 g photocatalyst alone and with the addition of IPA, TEOA or BQ.

photocatalytic experiments, which indicates that the construction of the 2D sheet heterostructure composite Bi/Nb-0.1 g is an efficient way to enhance visible light photocatalytic performance and improve the charge separation of photogenerated carriers.

To investigate the photodegradation mechanism of Bi/Nb-0.1 g, different appropriate species scavengers such as triethanolamine (TEOA),[45] isopropanol (IPA)[46] and benzoquinone (BQ)[47] were introduced into the MO solution prior to addition of the catalyst, as scavengers of photogenerated holes h^+, $^{\bullet}OH$ and $^{\bullet}O_2^-$, respectively. The final concentrations of TEOA, IPA and BQ in the reaction system were 1.0 mmol L^{-1}, 10 mmol L^{-1} and 1.0 mmol L^{-1}, respectively. The importance of the reactive species is proportional to the degradation rate of MO; in other words, compared to the result of the comparison experiment with no scavenger, the more the degradation rate of MO is reduced, the more important the role the reactive species plays in the reaction. Fig. 6b shows that TEOA and BQ dramatically suppressed the degradation of MO. However, the degradation rate of MO shows negligible reduction after the addition of IPA. The results reveal that photogenerated holes h^+ and $^{\bullet}O_2^-$ play important roles in the photodegradation of MO.

To further illuminate the photocatalytic mechanism of Bi/Nb-0.1 g, the valence band (VB) edge and conduction band (CB) edge positions of Bi_2OS_2 and Nb_6O_{17} were calculated empirically according to the formulas[48]

$$E^{\circ}_{VB} = X - E^{e} + 0.5E_g \quad (1)$$

$$E^{\circ}_{CB} = E^{\circ}_{VB} - E_g \quad (2)$$

$$E = E^{\circ} - 0.059\mathrm{pH} \quad (3)$$

where E_{VB} is the VB edge potential, and X is the electronegativity of the semiconductor. The electronegativity of the semiconductor is determined from the geometric mean of the electronegativities of the constituent atoms (the electronegativity of an atom is the arithmetic mean of the atomic electron affinity and the first ionization energy). E^e is the energy of free electrons on the hydrogen scale (about 4.5 eV), and E_g is the band gap energy of the semiconductor. The X values for Bi_2OS_2 and Nb_6O_{17} are calculated to be 5.77 and 6.39, and E_{VB} values for Bi_2OS_2 and Nb_6O_{17} were calculated to be 1.91 V and 3.64 V, respectively. Thus, the conduction bands (E_{CB}) of Bi_2OS_2 and Nb_6O_{17} were estimated to be 0.38 V and −0.09 V, respectively. Based on the calculated result above, we proposed a possible photocatalytic mechanism as illustrated in Scheme 2. Bi_2OS_2 with a narrow band gap energy (1.53 eV) can be easily excited by visible light (λ > 400 nm, energy less than 3.10 eV) and induce the generation of photoelectrons and holes. Furthermore, electrons in the VB of Bi_2OS_2 could also be photoexcited up to a higher potential edge (−1.19 V), due to the higher photon energy (3.10 eV). Nb_6O_{17} with a wide band energy (3.73 eV) cannot be excited by visible light (λ > 400 nm). Therefore, in the heterostructure of Bi/Nb-0.1 g, the reformed conduction band (CB) edge potential of Bi_2OS_2 is more active

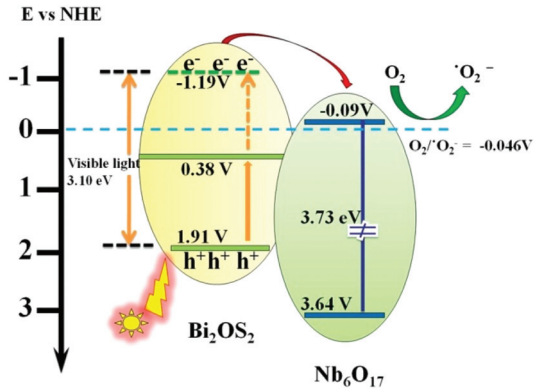

Scheme 2 Possible photocatalytic mechanism for the Bi/Nb-0.1 g composite.

than that of Nb_6O_{17} (−0.09 V). The excited electron on the surface of Bi_2OS_2 can easily transfer to Nb_6O_{17}, leaving holes in the valence band of Bi_2OS_2. This can be further confirmed through experiments on the photo-reduction of Pt (Fig. S5†). As shown in Fig. S5a,† after visible light irradiation, Pt nanoparticles were deposited on the Nb_6O_{17} sheets, which indicates the excited electrons were transferred from Bi_2OS_2 to the Nb_6O_{17} sheets. The separated electrons in the conduction band of Nb_6O_{17} combine with O_2 to produce radical $^{\bullet}O_2^-$. And the radical $^{\bullet}O_2^-$ and the holes can efficiently degrade the MO dye molecules. Therefore, the enhanced visible light photocatalytic performance of this 2D sheet composite Bi/Nb-0.1 g was observed as a result of the efficient separation of the photoexcited electrons and holes in the large interfacial heterostructure.

Conclusions

In summary, a series of 2D sheet $Bi_2O_xS_{3-x}/Nb_6O_{17}$ heterostructure photocatalysts were synthesized through a facile hydrothermal vulcanization method between Bi^{3+} exchanged $K_4Nb_6O_{17}$ and thiourea (NH_2CSNH_2). XRD and TEM results reveal that $Bi_2O_xS_{3-x}$ has been successfully intercalated into layers of $K_4Nb_6O_{17}$. The large interfacial contact between the layered $Bi_2O_xS_{3-x}$ and $K_4Nb_6O_{17}$ sheets is beneficial to the transfer and separation of photogenerated charge carriers. Thus the composite exhibits good photocatalytic performance for the degradation of methyl orange (MO) under visible light irradiation (λ > 400 nm), which is superior to that of both precursors, pure Bi_2S_3 and $K_4Nb_6O_{17}$. These 2D sheet composites might be one of the efficient and promising photocatalysts to be applied to wastewater purification and environmental remediation.

Acknowledgements

The authors gratefully acknowledge the financial support of the National Natural Science Foundation of China (grant no.

21271039, 21201032, 21401131, 21471028 and 21301166), Program for New Century Excellent Talents in University (grant no. NCET120813), Fundamental Research Funds for the Central Universities (grant no. 2412016KJ018, 11SSXT140) and Opening Project of Key Laboratory of Polyoxometalate Science of the Ministry of Education (grant no. 130014556).

Notes and references

1 W. Morales, M. Cason, O. Aina, N. R. Tacconi and K. Rajeshwar, *J. Am. Chem. Soc.*, 2008, **130**, 6318.
2 D. Rimeh, D. Patrick and R. Didier, *Ind. Eng. Chem. Res.*, 2013, **52**, 3581.
3 Z. Zou, J. Ye, K. Sayama and H. Arakawa, *Nature*, 2001, **414**, 625.
4 R. Asahi, T. Morikawa, T. Ohwaki, K. Aoki and Y. Taga, *Science*, 2001, **293**, 269.
5 Y. Qu and X. Duan, *Chem. Soc. Rev.*, 2013, **42**, 2568.
6 J. Zhang, Z. P. Zhu, Y. P. Tang, K. Mullen and X. L. Feng, *Adv. Mater.*, 2014, **26**, 734.
7 W. Wu, S. Zhang, F. Ren, X. Xiao, J. Zhou and C. Jiang, *Nanoscale*, 2011, **3**, 4676–4684.
8 M. Saruyama, Y.-G. So, K. Kimoto, S. Taguchi, Y. Kanemitsu and T. Teranishi, *J. Am. Chem. Soc.*, 2011, **133**, 17598–17601.
9 Y. Liu, L. Yu, Y. Hu, C. Guo, F. Zhang and X. W. D. Lou, *Nanoscale*, 2012, **4**, 183–187.
10 Y. Nonoguchi, T. Nakashima and T. Kawai, *Small*, 2009, **5**, 2403–2406.
11 X. H. Gao, H. B. Wu, L. X. Zheng, Y. J. Zhong, Y. Hu and X. W. Lou, *Angew. Chem., Int. Ed.*, 2014, **53**, 5917.
12 W. X. Guo, C. Xu, X. Wang, S. H. Wang, C. F. Pan, C. J. Lin and Z. L. Wang, *J. Am. Chem. Soc.*, 2012, **134**, 4437.
13 J. X. Low, S. W. Cao, J. G. Yu and S. Wageh, *Chem. Commun.*, 2014, **50**, 10768–10777.
14 K. Domen, A. Kudo, A. Shinozaki, A. Tanaka, K. Maruya and T. Onishi, *J. Chem. Soc., Chem. Commun.*, 1986, 356–357.
15 R. Z. Ma, Y. Kobayashi, W. J. Youngblood and T. E. Mallouk, *J. Mater. Chem.*, 2008, **18**, 5982–5985.
16 W. Q. Cui, Y. F. Liu, L. Liu, J. S. Hu and Y. H. Liang, *Appl. Catal., A*, 2012, 111–118.
17 Y. H. Liang, M. Y. Shao, L. Liu, J. G. McEvoy, J. S. Hua and W. Q. Cui, *Catal. Commun.*, 2014, **46**, 128–132.
18 W. Q. Cui, M. Y. Shao, L. Liu, Y. H. Lianga and D. Ranab, *Appl. Surf. Sci.*, 2013, **276**, 823–831.
19 W. Q. Cui, H. Wang, L. Liu, Y. H. Liang and J. G. McEvoyba, *Appl. Surf. Sci.*, 2013, **283**, 820–827.
20 W. Q. Cui, H. Wang, Y. H. Liang, B. X. Han, L. Liu and J. S. Hu, *Chem. Eng. J.*, 2013, **230**, 10–18.
21 W. Q. Cui, H. Wang, Y. H. Liang, L. Liu and B. X. Han, *Catal. Commun.*, 2013, **36**, 71–74.
22 K. Yao, S. Nishimura, Y. Imai, H. Wang, T. Ma, E. Abe, H. Tateyama and A. Yamagishi, *Langmuir*, 2003, **19**, 321–325.
23 N. Kimura, Y. Kato, R. Suzuki, A. Shimada, S. Tahara, T. Nakato, K. Matsukawa, P. H. Mutin and Y. Sugahara, *Langmuir*, 2014, **30**, 1169–1175.
24 W. W. Qu, F. Chen, B. Zhao and J. L. Zhang, *J. Phys. Chem. Solids*, 2010, **71**, 35–41.
25 J. J. Ma, J. Wu, J. Z. L. Liu, D. G. Zhang, X. Y. Xu, X. J. Yang and Z. W. Tong, *Mater. Lett.*, 2012, **71**, 4–6.
26 K. Mori, S. Ogawa, M. Martis and H. Yamashita, *J. Phys. Chem. C*, 2012, **116**, 18873–18877.
27 H. Cheng, B. Huang and Y. Dai, *Nanoscale*, 2014, **6**, 2009–2026.
28 L. S. Zhang, W. Z. Wang, L. Zhou and H. Xu, *Small*, 2007, **3**, 1618–1625.
29 L. S. Zhang, H. L. Wang, Z. G. Chen, P. K. Wong and J. S. Liu, *Appl. Catal., B*, 2011, **106**, 1–13.
30 L. Zhang, T. Xu, X. Zhao and Y. Zhu, *Appl. Catal., B*, 2010, **98**, 138–146.
31 W. Yin, W. Wang and S. Sun, *Catal. Commun.*, 2010, **11**, 647–650.
32 Y. Shimodaira, H. Kato, H. Kobayashi and A. Kudo, *J. Phys. Chem. B*, 2006, **110**, 17790–17797.
33 Y. Ma, Y. Jia, Z. Jiao, M. Yang, Y. Qi and Y. Bi, *Chem. Commun.*, 2015, **51**, 6655–6658.
34 J. Long, S. Wang, H. Chang, B. Zhao, B. Liu, Y. Zhou, W. Wei, X. Wang, L. Huang and W. Huang, *Small*, 2014, **10**, 2791–2795.
35 Z. Li, X. Chen and Z. Xue, *CrystEngComm*, 2013, **15**, 498–508.
36 M. Zhang, C. Shao, P. Zhang, C. Su, X. Zhang, P. Liang, Y. Sun and Y. Liu, *J. Hazard. Mater.*, 2012, **225**, 155–163.
37 R. Li, F. Zhang, D. Wang, J. Yang, M. Li, J. Zhu, X. Zhou, H. Han and C. Li, *Nat. Commun.*, 2013, **4**, 1432.
38 X. Zhang, Y. F. Liu, G. H. Zhang, Y. Q. Wang, H. Zhang and F. Q. Huang, *ACS Appl. Mater. Interfaces*, 2015, **7**, 4442–4448.
39 L. Tian and H. Y. Tan, *Cryst. Growth Des.*, 2008, **8**, 734.
40 Y. Y. Zhang, Y. P. Guo, B. J. Fang, Y. J. Chen, H. N. Duan, H. Lia and H. Z. Liu, *Appl. Catal., A*, 2016, **514**, 146–153.
41 J. F. Moulder, W. F. Sticke, P. E. Sobol and K. D. Bomben, *Handbook of X-Ray Photoelectron Spectroscopy*, Perkin-Elmer Corp, USA, 1992.
42 V. I. Nefedov, D. Gati, B. F. Dzhurinskii, N. P. Sergushin and Y. V. Salyn, *Zh. Neorg. Khim.*, 1975, **20**, 2307.
43 M. A. B. Gomes, L. O. de S. Bulhoes, S. C. de Castro and A. J. J. Damiao, *Electrochem. Soc.*, 1990, **137**, 3067.
44 J. P. Contour, G. Mouvier, M. Hoogewijs and C. J. Leclere, *Catalysis*, 1977, **48**, 217.
45 N. Aman, T. Mishra, J. Hait and R. K. Jana, *J. Hazard. Mater.*, 2011, **186**, 360–366.
46 T. G. Xu, L. W. Zhang, H. Y. Cheng and Y. F. Zhu, *Appl. Catal., B*, 2011, **101**, 382.
47 H. W. Huang, K. Liu, K. Chen, Y. L. Zhang, Y. H. Zhang and S. C. Wang, *J. Phys. Chem. C*, 2014, **118**, 14379.
48 M. L. Guan, D. K. Ma, S. W. Hu, Y. J. Chen and S. M. Huang, *Inorg. Chem.*, 2011, **50**, 800.

